

Characterization of *Trypanosoma brucei* dihydroorotate dehydrogenase as a possible drug target; structural, kinetic and RNAi studies

Tracy L. Arakaki,^{1,2†} Frederick S. Buckner,^{2,3†}
J. Robert Gillespie,³ Nicholas A. Malmquist,⁴
Margaret A. Phillips,⁴ Oleksandr Kalyuzhnyi,^{1,2}
Joseph R. Luft,^{2,5} George T. DeTitta,^{2,5}
Christophe L. M. J. Verlinde,^{1,2}
Wesley C. Van Voorhis,^{2,3} Wim G. J. Hol,^{1,2} and
Ethan A. Merritt^{1,2*}

¹Departments of Biochemistry and ³Medicine, University of Washington, Seattle, WA 98195, USA.

²Structural Genomics of Pathogenic Protozoa (SGPP), <http://www.sgpp.org>.

⁴Department of Pharmacology, University of Texas Southwestern Medical Center, Dallas, TX 75390, USA.

⁵Hauptman Woodward Institute, Buffalo, NY, USA.

Summary

Nucleotide biosynthesis pathways have been reported to be essential in some protozoan pathogens. Hence, we evaluated the essentiality of one enzyme in the pyrimidine biosynthetic pathway, dihydroorotate dehydrogenase (DHODH) from the eukaryotic parasite *Trypanosoma brucei* through gene knockdown studies. RNAi knockdown of DHODH expression in bloodstream form *T. brucei* did not inhibit growth in normal medium, but profoundly retarded growth in pyrimidine-depleted media or in the presence of the known pyrimidine uptake antagonist 5-fluorouracil (5-FU). These results have significant implications for the development of therapeutics to combat *T. brucei* infection. Specifically, a combination therapy including a *T. brucei*-specific DHODH inhibitor plus 5-FU may prove to be an effective therapeutic strategy. We also show that this trypanosomal enzyme is inhibited by known inhibitors of bacterial Class 1A DHODH, in distinction to the sensitivity of DHODH from human and other higher eukaryotes. This selectivity is supported by the crystal structure of the *T. brucei* enzyme, which is reported here at a

resolution of 1.95 Å. Additional research, guided by the crystal structure described herein, is needed to identify potent inhibitors of *T. brucei* DHODH.

Introduction

Pyrimidine biosynthesis is a vital biological process, achieved both by *de novo* synthesis and by pyrimidine salvage pathways. However, many parasitic protozoa are deficient in pyrimidine salvage (Chaudhary and Roos, 2005) and thus enzymes of the pyrimidine synthesis pathway have been considered potential drug targets. The fourth enzyme of this pathway is dihydroorotate dehydrogenase (DHODH), which oxidizes dihydroorotate to orotate, the first aromatic intermediate in this pathway, with consequent transfer of two electrons to the protein cofactor FMN (Fig. 1). Recent experiments to validate DHODH as a drug target in *Trypanosoma cruzi* showed that insect stage epimastigotes are dependent on *de novo* synthesis of pyrimidines (Annoura *et al.*, 2005). Specifically, gene interruption of the three gene loci encoding cytosolic DHODH in *T. cruzi* led to cell non-viability; addition of pyrimidine nucleosides to the medium did not rescue the DHODH knockdown cells. We therefore undertook a more extensive investigation of the essentiality of the closely homologous gene in *T. brucei*, the causative agent of African Sleeping Sickness.

Dihydroorotate dehydrogenases are categorized into two classes, Class 1 and Class 2, based upon their sequence, localization in the cell, and the electron acceptor used to reoxidize FMN in a second half-reaction (Nielsen *et al.*, 1996a, b). Both classes belong to Pfam sequence family PF01180. Class 1 DHODHs are primarily bacterial. They are cytosolic and further divided into 1A (E.C. 1.3.3.1) and 1B (E.C. 1.3.1.14) depending upon their electron acceptor and oligomeric state. Class 2 DHODHs, including the human and plasmodial enzymes, are monomeric and contain mitochondrial targeting sequences located in the N-terminal domain (Rowland *et al.*, 2000). Furthermore, they are found in the inner membrane of mitochondria (Knecht *et al.*, 1996) or associated with the cytoplasmic membranes in the case of *Escherichia coli* (Karibian, 1978). Specific inhibitors are

Accepted 14 January, 2008. *For correspondence. E-mail merritt@u.washington.edu; Tel. (+1) 206 543 1421; Fax (+1) 206 685 7002. †Contributed equally.

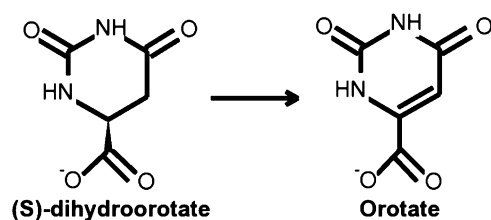


Fig. 1. Oxidation of dihydroorotate to orotate.

known for both classes (Palfey *et al.*, 2001; Baldwin *et al.*, 2005).

We present genomic, biochemical and structural evidence that TbDHODH is a Class 1A DHODH, and in particular that it can be inhibited by Class 1A specific inhibitors. The structural analysis is based on a 1.95 Å resolution crystal structure of the *T. brucei* enzyme co-crystallized with the reaction product orotate. We also present kinetic, inhibition, biophysical and RNAi knock-down data for the *T. brucei* DHODH, which has not previously been characterized. Furthermore, we show that RNAi knockdown of *T. brucei* DHODH is synergistic with the effects of 5-fluorouracil (5-FU), an inhibitor of pyrimidine uptake in *T. brucei* (de Koning and Jarvis, 1998). This finding provides a rationale to develop DHODH inhibitors that could be used in combination with 5-FU or another inhibitor of pyrimidine uptake to yield a potent therapeutic regimen. We are encouraged that the structure and inhibition studies offer insight into the stereochemical and functional details of the active site of the trypanosomal enzyme, and may facilitate the development of lead compounds for antitrypanosomal drug discovery. Because our results on the essentiality of this enzyme are divergent from those reported for the closely related *T. cruzi* parasite, they also underscore the importance of validating antiprotozoan drug targets separately in each target organism (Wang, 1997).

Results

Only one DHODH gene was found in the *T. brucei* genome (GeneDB Tb927.5.3830). This gene was initially identified as a structural genomics target (TargetDB Tbru015978) by the Structural Genomics of Pathogenic Protozoa consortium (SGPP). At the time this work was initiated no trypanosomal DHODH structures were available, although a preliminary characterization of *Leishmania major* DHODH had been presented (Feliciano *et al.*, 2006) and preliminary crystallization of the *T. cruzi* enzyme had been reported (Inaoka *et al.*, 2005). Thus we undertook *de novo* crystallographic structure determination of the *T. brucei* DHODH, and also undertook biochemical characterization of this enzyme to confirm the assignment of the trypanosomal enzymes to Class 1A.

Structural analysis

The crystal structure of TbDHODH was determined to 1.95 Å resolution from a single crystal in space group C222₁. Consistent with previously determined structures from this sequence family, the overall fold of the TbDHODH monomer is an $\alpha\beta$ barrel with the prosthetic FMN group located near the C-terminus (Fig. 2A).

The asymmetric unit of the crystal structure contains four monomers that are arranged as two distinct dimers. The monomers of each dimer are related by twofold symmetry and the dimer overlays well with the *Lactococcus lactis* 1A dimer. The area of contact at the dimer interface of is 2300 Å² as analysed by PDBsum (Laskowski *et al.*, 2005). The interface includes 19 inter-monomer hydrogen bonds and a salt bridge between Glu-208 of monomer A and Lys-297 of monomer B. This salt bridge is also observed in the *L. lactis* structure. Lys-297 is strictly conserved among Class 1A DHODHs; residue 208 is conserved as either glutamate or aspartate (Fig. S2). Thus, this salt bridge is a characteristic feature of the dimer interface in Class 1A DHODHs.

The oligomeric state of the protein was also examined by analytical ultracentrifugation. TbDHODH was observed by both protein absorption at 280 nm and FMN absorption at 454 nm. Throughout centrifugation experiments, a single ideal species model consistently yielded an average mass indicative of a dimeric enzyme, while a monomer/dimer model reliably produced submicromolar dissociation constants for dimerization (Fig. S1). This biophysical result supports the crystallographic observation of TbDHODH as a homodimer.

The TbDHODH structure contains two *cis*-peptides, Glu-56–Pro-57 and Cys-193–Val-194. These *cis*-peptides are also observed in structures of the *L. lactis* 1A, *L. lactis* 1B and human Class 2 homologues. The two residues following the first *cis*-peptide, Arg58 and Tyr59, are in close proximity to the active site and are highly conserved among Class 1A DHODH sequences. No other exceptional stereochemistry is observed in the refined TbDHODH model.

FMN binding site

The FMN prosthetic group is located near the dimer interface in a pocket formed predominantly by strands β 4, β 6–7, β 11 and β 17. FMN forms hydrogen bonds with residues Ala-20, Ser-45, Lys-44, Cys-249, Val-194 and Lys-165 (Fig. S3); and hydrophobic interactions with residues Ala-19, Gly-21, Met-70, Tyr-59, Asn-68 and with orotate. The isoalloxazine ring of FMN and the aromatic ring of orotate are parallel to each other as in other DHODH-orotate structures. The dimethylbenzene moiety of the isoalloxazine ring system lacks close contacts to

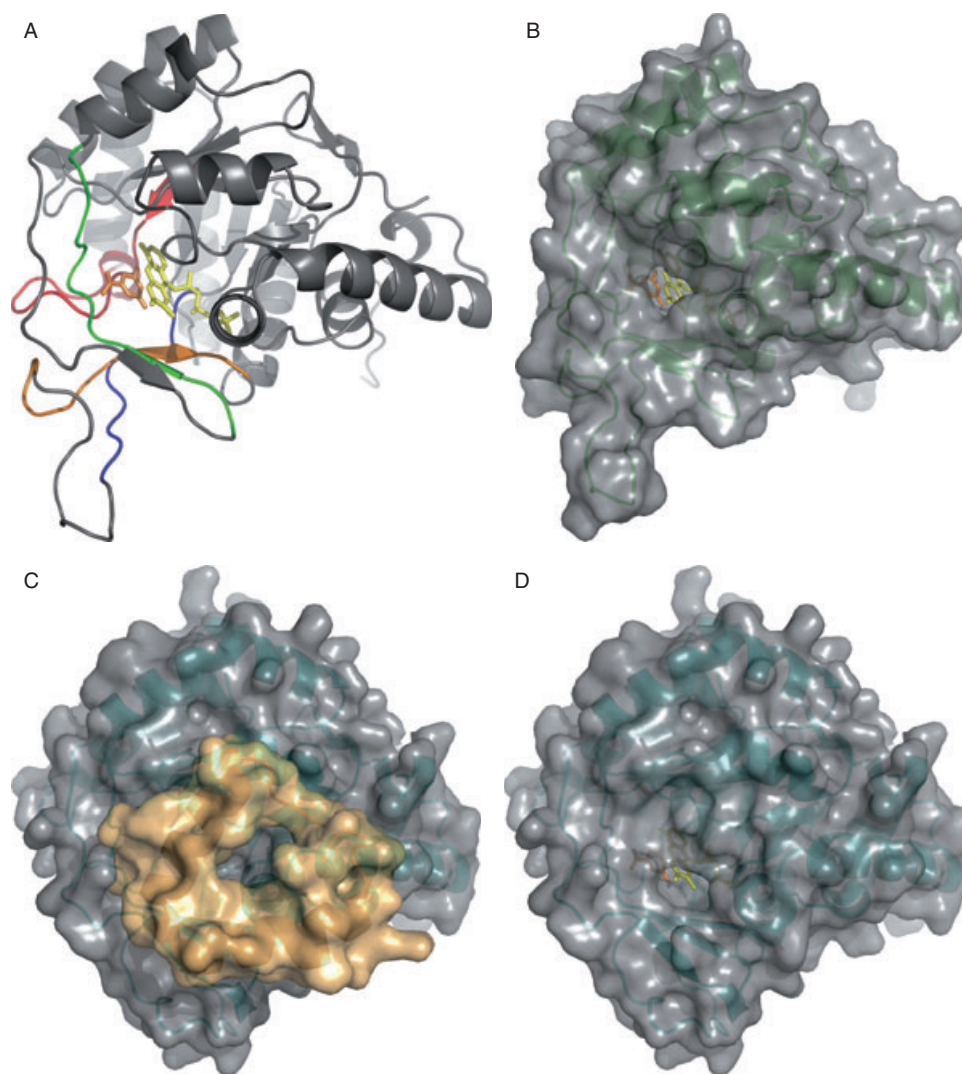


Fig. 2. Comparison of *T. brucei* and human DHODH. TbDHODH is homodimeric, typical of Class 1A homologues. The human enzyme is monomeric, characteristic of Class 2 homologues.

A. TbDHODH monomer showing Class 1A motifs: Motif 1 (residues 195–203, blue), Motif 2 (residues 64–76, green), Motif 3 (residues 214–223, orange), Pyr-binding motif (residues 126–143, red). The orotate and FMN cofactors are shown in brown and yellow respectively.

B. Surface representation of TbDHODH, showing that the orotate and FMN sites are relatively solvent accessible even with loop 132–138 in a 'closed' conformation.

C. Surface representation of the entire human DHODH monomer including well-ordered residues (30–69) from the N-terminal domain (brown). In Class 2 homologues the N-terminal domain restricts solvent access to the orotate and FMN binding sites from this direction. The depression visible at the centre of the surface is the binding site for the Class 2 DHODH redox partner ubiquinone, and for Class 2 specific inhibitors such as brequinar.

D. Surface representation the human DHODH with N-terminal residues removed for the purpose of comparison to the trypanosomal enzyme.

any residue and is solvent accessible. This differs from the FMN binding site in the human structure (25% sequence identity), where the Class 2-specific N-terminal domain blocks access to the active site. There are similar hydrogen bonding interactions to the FMN in both the TbDHODH and human structures and these residues are conserved between the two structures except for Lys-44 and Cys-249. The sulphhydryl of Cys-249 forms a hydrogen bond to O3 of the ribityl group of FMN. The equivalent interaction is absent in the human structure, where there

is only one hydrogen bond to O3. In a sequence-based structure alignment, Lys-44 is a glycine in the human structure but there is a nearby lysine (hLys-100), which forms hydrogen bonds to O4 of the isoalloxazine ring and plays the same role in binding to FMN. Of the five residues in TbDHODH that form hydrophobic interactions to FMN, two are different in the human protein. These differences may be of potential use in designing an inhibitor targeting the FMN binding site with differential specificity for the human and trypanosomal enzymes.

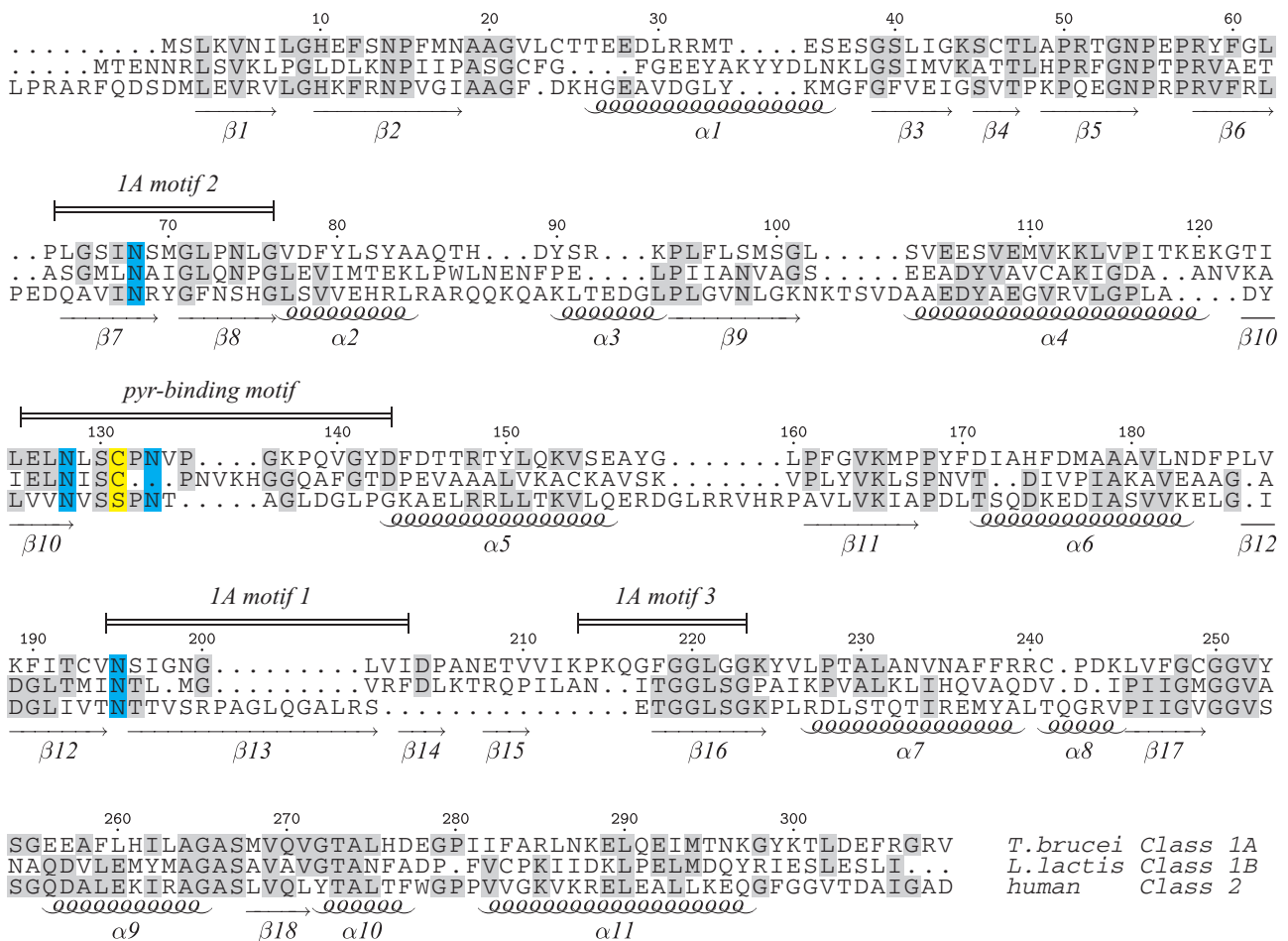


Fig. 3. A structure-based sequence alignment of the Class 1A *T. brucei* (current structure), the Class 1B *L. lactis* (PDB accession code 1ep1), and the Class 2 human DHODH (PDB accession code 1d3g). The active site Cys-131 is coloured yellow. Four Asn residues important for catalysis and conserved in all classes of DHODH are coloured cyan. Three Class 1A motifs that may further aid in the classification of DHODHs are labelled and further discussed in Fig. S2. Residue numbering and secondary structure elements correspond to the *T. brucei* DHODH. The alignment was generated using the CEMC Multiple Protein Structure Alignment Server (<http://bioinformatics.albany.edu/~cemc/>) (Guda *et al.*, 2004) and coloured using T_xShade (Beitz, 2000). The human sequence shown begins at residue 69, omitting the N-terminal domain that is not present in the Class 1 homologues.

Orotate binding site and conserved motifs in Class 1A DHODH

Class 1 and Class 2 DHODHs differ at the active site base responsible for the abstraction of a proton from the C5 of orotate. In Class 1A DHODHs the base is a cysteine; in Class 2 enzymes, including human DHODH, it is a serine (Nørager *et al.*, 2003). In TbDHODH, S^γ of the active site base Cys-131 is 3.65 Å away from C5 of orotate. This distance is slightly longer than the 3.3 Å observed in the *L. lactis* DHODH:orotate structure. In the present crystal structure at pH 4 the cysteine sulphur is most likely protonated. Residues 126–143, spanning the region to either side of the active site Cys, are strongly conserved among all Class 1A DHODHs (Fig. S2). These residues can be described as a pyrimidine binding motif: EZNLSCP NZPUKZQXXYD, where U is a polar

uncharged residue, X is a non-specific residue and Z is a hydrophobic residue.

A structure-based sequence alignment of the *T. brucei*, *L. lactis* 1B, and human DHODHs, representing Classes 1A, 1B and 2, respectively, shows that the Class 1 sequences have an insertion of 15 residues (residues 202–216) relative to the human Class 2 sequence (Fig. 3). These residues form a strand-loop–strand-loop (β14-loop–β15-loop) structural unit. Residues 195–203 preceding the insertion are conserved among Class 1A DHODHs and form a NSXGNLXI motif (1A motif 1) in close proximity to the active site. Asn-195 is one of four conserved Asn residues that interact with orotate.

The orotate binding site is flanked by a loop consisting of residues 132–138 (Fig. S4). This loop is highly conserved in Class 1A DHODHs (Fig. S2). In crystal structures of human DHODH the corresponding loop is poorly

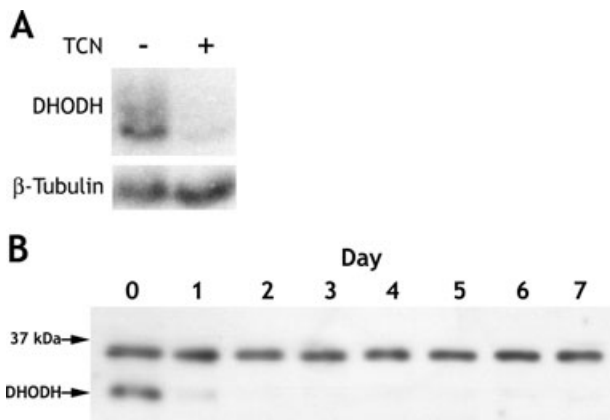


Fig. 4. Knockdown of DHODH mRNA expression (A) and DHODH protein expression (B) after induction of RNAi with tetracycline. (A – top) Northern blot of *T. brucei* cells collected 72 h post tetracycline induction of RNAi (TCN+) demonstrates 95% knockdown of DHODH mRNA compared with cells containing the same construct with RNAi uninduced (TCN-). (A – bottom) β -tubulin mRNA expression levels show near-equivalent RNA loading. (B) A Western blot was performed on cell lysates collected on day 0 (preinduction) through 7 days post induction. The blot was probed with an anti-*T. brucei* DHODH antibody. The upper band represents binding to an unidentified protein that is not affected by the RNAi expression. The predicted DHODH protein is labelled and is nearly absent 1 day after induction of RNAi.

ordered, and loop flexibility is hypothesized to allow the active site to open so that dihydroorotate can enter and orotate can exit (Liu *et al.*, 2000). In contrast to the human structure, the loop in the present TbDHODH structure is in a relatively closed conformation and is well defined by electron density. Nevertheless, the orotate and FMN binding sites are more accessible in TbDHODH than in the human structure owing to the absence of the N-terminal domain characteristic of Class 2 DHODH (Fig. 2). This difference in accessibility may contribute to the differential sensitivity of the Class 1A and Class 2 enzymes to orotate analogues such as hydroxybenzoate.

RNA interference studies of *T. brucei* DHODH

Gene expression knockdown of the *T. brucei* DHODH was achieved by overexpressing a stem-loop RNA of the target gene in bloodstream form *T. brucei*. Messenger RNA levels were decreased by 95% at 72 h following induction of the RNA interference construct by the addition of tetracycline (Fig. 4A). Knockdown of *T. brucei* DHODH protein appeared to be similarly substantial as observed on Western blots. This was monitored over 7 days, with protein levels detected at < 5% of levels observed without RNAi induction (Fig. 4B). When the *T. brucei* cells were grown in standard medium (HMI-9), growth rates for cells when RNAi was turned on (TCN+) or turned off (TCN-) were comparable (Fig. 5A). The growth rates of these cultures were virtually the same as the

control cells ('single-marker') containing only the T7 RNA polymerase and Tet repressor genes maintained on a neomycin marker. The surprising observation of normal cell growth led us to investigate if the parasites were

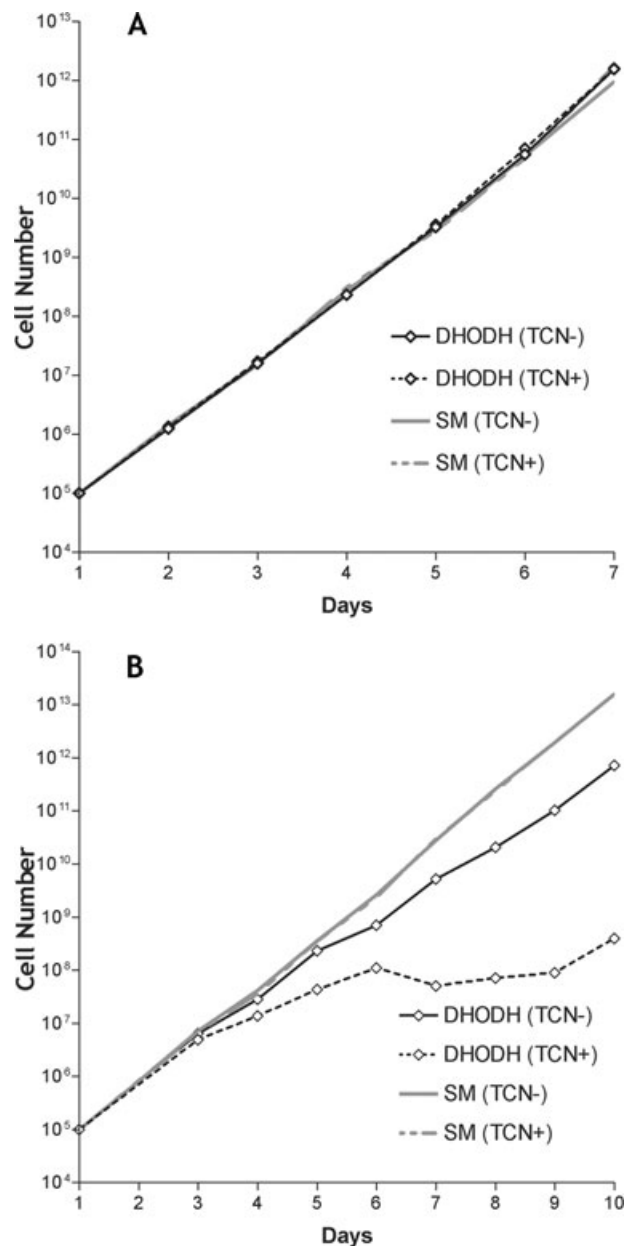


Fig. 5. Gene knockdown of *T. brucei* DHODH using RNA interference. Cumulative cell densities are shown on a log-scale as the product of the cell number and the total dilution. A. Cell growth was monitored of *T. brucei* undergoing RNAi of DHODH (TCN+) and compared with cells without RNAi induction (TCN-). The cells were grown in standard media for bloodstream form *T. brucei*. The growth rate was also compared with the 'single marker' (SM) strain of *T. brucei* that was not transfected with the RNAi expression vector (semi-logarithmic plot). B. The same experiment as in A was repeated using pyrimidine-depleted medium.

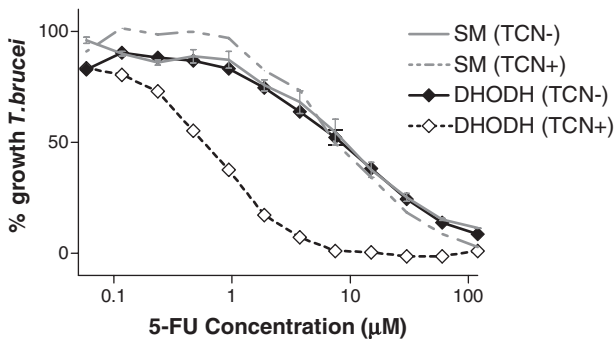


Fig. 6. Effects of different concentrations of 5-FU on *T. brucei* cells. RNAi was induced with tetracycline for 48 h, then cells were incubated with serial dilutions of 5-FU for another 48 h before being quantified with Alamar Blue. Labelling is the same as in Fig. 5.

surviving by scavenging pyrimidines from the medium. Note that HMI-9 medium includes 16 μM thymidine. When the additional thymidine was omitted from the medium, we again saw no change in the growth phenotype upon induction of RNA interference against the DHODH (data not shown). As the standard medium was made up with 10% fetal bovine serum, we repeated the experiment using commercially available dialysed serum, which was depleted of small molecules such as pyrimidines. Under these conditions we observed reduced growth upon induction of the RNAi construct. By day 4 the growth rate was significantly reduced and was arrested by day 6 (Fig. 5B). Most of the cells expressing the RNAi construct in the pyrimidine-depleted medium took on a bloated, balloon-shaped morphology by day 5. There was a small degree of growth suppression in the TCN⁻ cells compared with the single-marker controls, which may have been due to leaky expression of the RNAi construct.

We therefore proceeded to test whether RNAi knock-down of DHODH would impair growth in standard medium if an inhibitor of pyrimidine uptake were also present. 5-FU was tested as it has been shown to be a potent inhibitor of pyrimidine uptake by *T. brucei* (Gudin *et al.*, 2006). The inhibitory concentration of 5-FU causing 50% growth inhibition (IC_{50}) was shifted 16-fold lower in parasites undergoing knockdown of DHODH ($\text{IC}_{50} = 0.64 \mu\text{M}$) compared with parasites not undergoing knockdown ($\text{IC}_{50} = 10.4 \mu\text{M}$) using standard medium (Fig. 6). In follow-up to this finding, we tested the uptake of ^3H -5-FU into the DNA of *T. brucei* cells and observed that uptake was more than twofold higher in the DHODH-knockdown parasites than in controls (Fig. 7).

Classification of TbDHODH as Class 1A and inhibition by hydroxybenzoates

TbDHODH activity was examined in the presence of several standard DHODH terminal electron acceptors

(Fig. 8) and was found to catalyse fumarate most efficiently, typical of Family 1A enzymes (Andersen *et al.*, 1994). The enzyme catalyses the reduction of menadiene (vitamin K_3) at $\sim 20\%$ the rate of fumarate catalysis, but does not appear to perform electron transfer to menaquinone (vitamin K_2), to the ubiquinone analogues Q_0 , Q_1 , Q_2 , or Q_D , or to NAD^+ , further characteristics of a Family 1A DHODH enzyme (Nielsen *et al.*, 1996a; Marcinkeviciene *et al.*, 2000; Nara *et al.*, 2000). Catalysis of both DHO and fumarate displays saturation kinetics with K_m values of 14 μM for DHO and 80 μM for fumarate and a $k_{\text{cat}}^{\text{app}}$ of 8.5 s^{-1} (Fig. 9). The pH dependence of enzyme activity was assayed (Fig. 9 inset) and peak activity was found to occur at pH 7.8, indicative of two ionizable groups with pK_a values of 6.3 and 9.2 being involved in substrate binding and catalysis. Analysis of

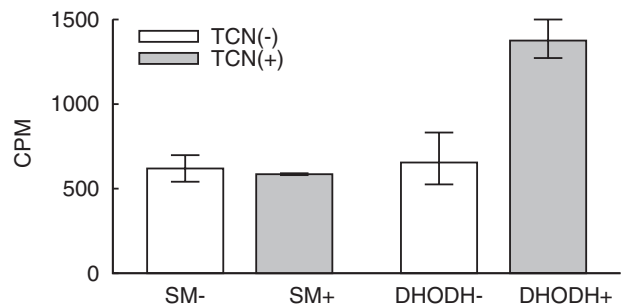


Fig. 7. Incorporation of ^3H -5-FU into *T. brucei* cells. RNAi was induced with tetracycline for 72 h, then cells were exposed to ^3H -5-FU for an additional 24 h before harvesting and quantifying tritium uptake into DNA. Labelling is the same as in Fig. 5. CPM, counts per minute.

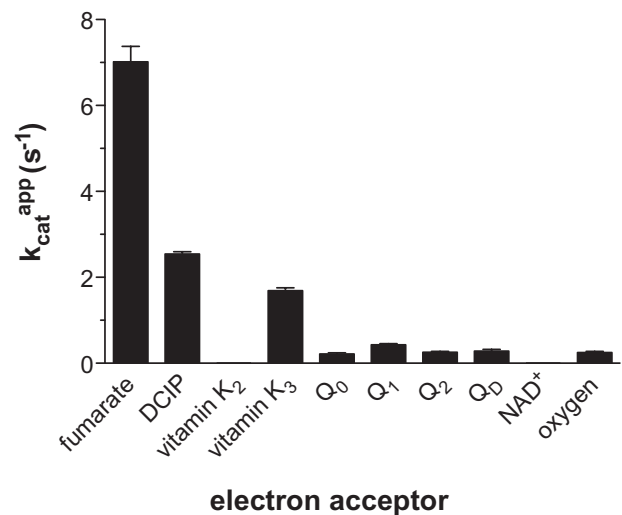


Fig. 8. Terminal electron acceptor preference of TbDHODH. Activity was examined in the presence of 250 μM DHO and 100 μM electron acceptor or $\sim 210 \mu\text{M}$ molecular oxygen. The $k_{\text{cat}}^{\text{app}}$ is the apparent k_{cat} obtained at a fixed concentration of both DHO (0.25 mM) and oxidant.

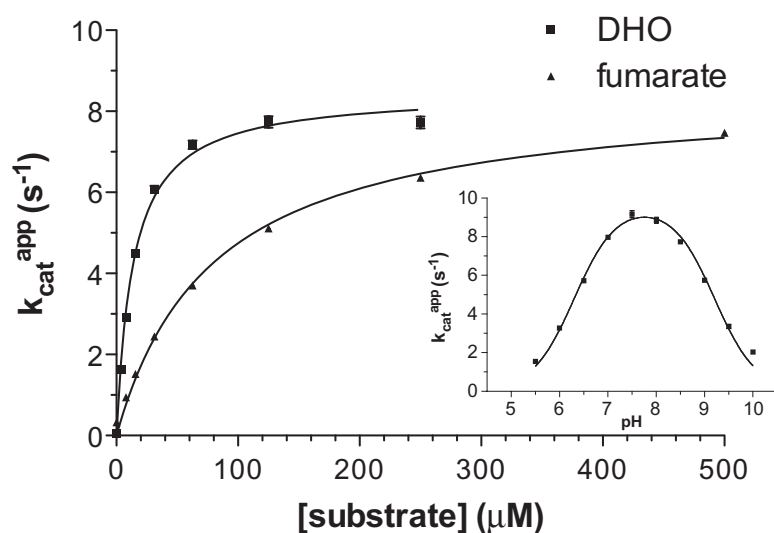


Fig. 9. Saturation kinetics of *T. brucei* DHODH toward DHO and fumarate. DHO-dependent activity was assayed in the presence of 500 μM fumarate and fumarate-dependent activity was assayed in the presence of 250 μM DHO at pH 8. $k_{\text{cat}}^{\text{app}}$ is 8.5 s^{-1} , K for DHO is 14 μM , K_{m} for fumarate is 80 μM . The $k_{\text{cat}}^{\text{app}}$ is the apparent k_{cat} obtained at a fixed concentration of one substrate while the other is varied. Inset: pH-dependent *T. brucei* DHODH activity. Activity was determined in the presence of 125 μM DHO and 500 μM fumarate. Activity peaks at pH 7.8 and the curve indicates two ionizable groups with $\text{p}K_{\text{a}}$ values of 6.3 and 9.2.

TbDHODH activity across a range of DHO and fumarate concentrations produces a double-reciprocal plot with parallel lines (Fig. 10), indicative of a ping-pong mechanism and consistent with results found for other Family 1A enzymes (Marcinkeviciene *et al.*, 2000).

Inhibition of TbDHODH by benzoate pyrimidine analogues was initially performed with 1 mM inhibitor (data not shown). Of the benzoate pyrimidine analogues tested, only 3,4- and 3,5-dihydroxybenzoate displayed inhibition at 1 mM concentration. Subsequent analysis of TbDHODH inhibition by 3,4- and 3,5-dihydroxybenzoate across various inhibitor and DHO concentrations (Fig. 11) revealed competitive inhibition by 3,4-dihydroxybenzoate with a K_{i} of ~ 58 μM (determined by IC_{50} re-plot, not shown) and weaker inhibition by 3,5-dihydroxybenzoate, which appeared non-competitive and yielded a K_{i} of 200 μM . These values are comparable to that reported for other Class 1A DHODHs (Takashima *et al.*, 2002; Feliciano *et al.*, 2006).

Discussion

Divergent pyrimidine requirement in T. cruzi and T. brucei

The *Trypanosoma brucei* genome contains all of the enzymes required for *de novo* pyrimidine biosynthesis, indicating that *T. brucei* is capable of providing its own pyrimidine pools (Berriman, 2004). The fourth enzyme in the pathway, DHODH, has been considered a potential drug target in parasitic protozoa including *Plasmodium falciparum* and *T. cruzi* (McRobert and McConkey, 2002; Annoura *et al.*, 2005; Baldwin *et al.*, 2005). In particular, the Class 1A DHODH from *T. cruzi* has been shown by gene disruption experiments to be necessary for growth of epimastigotes (Annoura *et al.*, 2005). We performed functional, enzymatic, and structural studies of this protein in the related parasite *T. brucei*, the causative agent of African sleeping sickness, in an attempt to confirm similar essentiality.

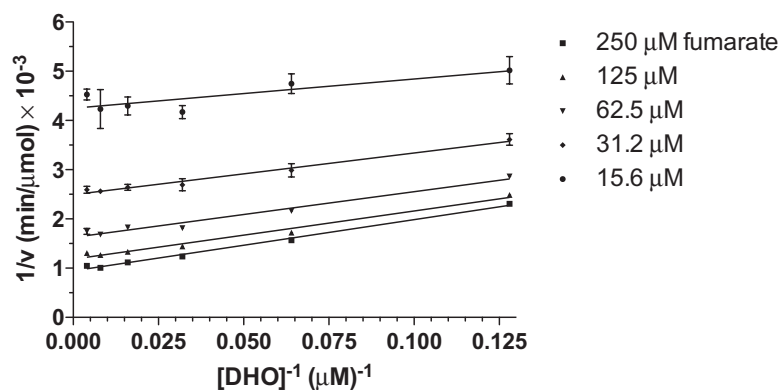


Fig. 10. Ping-pong kinetics of *T. brucei* DHODH. Double-reciprocal plot of DHO-dependent activity in the presence of varying concentrations of fumarate and 5 nM *T. brucei* DHODH produce parallel lines indicative of a ping-pong enzyme mechanism.

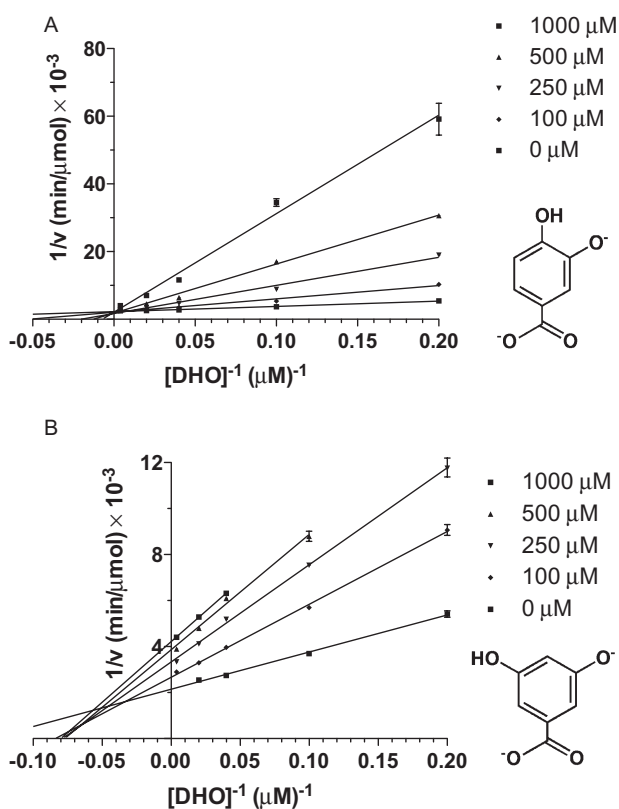


Fig. 11. Inhibition of TbDHODH by 3,4- or 3,5-dihydroxybenzoate. Activity was determined at varying concentrations of DHO and inhibitor and 5 nM *T. brucei* DHODH. Double reciprocal plots show characteristic competitive inhibition by the indicated concentrations 3,4 dihydroxybenzoate (A) and non-competitive inhibition by 3,5 dihydroxybenzoate (B).

Functional studies using RNA interference to block TbDHODH revealed that bloodstream *T. brucei* are able to grow normally without this enzyme, apparently by scavenging pyrimidines from the medium (Fig. 5). This ability to scavenge pyrimidines is not entirely unexpected, as it has been shown that *T. brucei* has surface transporters capable of importing uracil and cytosine (de Koning and Jarvis, 1998; Papageorgiou *et al.*, 2005; Gudin *et al.*, 2006). In addition, the *T. brucei* genome contains at least some of the enzymes associated with pyrimidine salvage, including cytidine deaminase (GeneDB Tb09.160.1680), uracil phosphoribosyltransferase (GeneDB Tb927.4.3320), and thymidine kinase (GeneDB Tb10.70.7270).

Thus, for *T. brucei*, a chemotherapeutic strategy to deprive the cells of pyrimidine pools would appear to require both inhibition of pyrimidine biosynthesis and of pyrimidine uptake/salvage. We tested the feasibility of such a two-pronged attack by repeating the DHODH RNAi knockdown experiments in the presence of 5-FU, a compound previously demonstrated to inhibit pyrimidine uptake by *T. brucei* (Gudin *et al.*, 2006). 5-FU is itself

cytotoxic at high concentrations owing to inhibition of thymidylate synthase and incorporation into DNA and RNA (de Bono and Twelves, 2001). We observed that cells undergoing this dual treatment were indeed affected by DHODH knockdown, and were 16-fold more sensitive to 5-FU than control cells (Fig. 6). This suggests that the cells could not tolerate both inhibition of pyrimidine synthesis and inhibition of pyrimidine uptake.

Although 5-FU inhibits pyrimidine uptake in *T. brucei*, it is itself transported into the cells with relatively high efficiency (Gudin *et al.*, 2006). A possible cellular response to the suppression of pyrimidine biosynthesis, in this case through interference with DHODH, is to upregulate the import pathway. Thus, a follow-up experiment was performed to determine the relative uptake of radiolabelled 5-FU into the DNA of the *T. brucei* cells in the presence or absence of DHODH suppression. The experiment demonstrated $> 2\times$ higher 5-FU incorporation into DHODH knockdown cells than into controls (Fig. 7). It seems likely that the increased incorporation of 5-FU into DNA could partly account for the enhanced sensitivity to this drug. We speculate that the increased incorporation of 5-FU into the DNA of DHODH knockdown cells results from one or more of the following factors: (i) the depletion of intracellular pyrimidine pools favours the incorporation of the 5-FU; (ii) possible upregulation of enzymes that convert 5-FU to 5-FU monophosphate, 5-FU diphosphate or 5-FU triphosphate; and (iii) possible increased uptake of 5-FU owing to upregulated pyrimidine transporter activity at the cell surface. Future experiments will be necessary to better establish if any of these mechanisms are responsible for our observations.

Whichever of the above mechanisms may be in play, the apparent synergy of DHODH knockdown plus 5-FU treatment has significant implications for pursuing the pyrimidine biosynthesis pathway as a drug target in *T. brucei*. One can imagine a combination treatment including 5-FU and a new compound that specifically inhibits the *T. brucei* DHODH (or possibly another enzyme in the pyrimidine biosynthesis pathway). A new DHODH inhibitor would thus be a 'chemosensitizer' for 5-FU and could dramatically enhance the activity of 5-FU for treating *T. brucei* infection. 5-FU is a well-established clinical drug that has been in use since the 1950s. It has known toxicities, but certainly has many advantages over existing human African trypanosomiasis drugs (e.g. melarsoprol, suramin, pentamidine, etc.) that are extremely toxic or require parenteral administration. It would be important to develop a partner drug that inhibits the *T. brucei* DHODH selectively. As the human DHODH is a Class 2 enzyme and thus functionally and structurally distinct from the Class 1 *T. brucei* enzyme, we expect that finding selective inhibitors is quite feasible. The data presented here provide a strong rationale for further pursuing

research into the *T. brucei* DHODH in order to develop potent inhibitors as drug leads.

Inhibitors of trypanosomal Class 1A DHODH

The previous focus of inhibitor studies has largely been directed to Class 2 DHODHs. The *P. falciparum* enzyme (PfDHODH) is the focus of significant interest for its potential as a new target for the development of antimalarials (Baldwin *et al.*, 2005), and the human enzyme is targeted for treatment of cancer, gastric ulcers and rheumatoid arthritis (Palfey *et al.*, 2001). Structural studies of PfDHODH inhibitors based upon brequinar analogues (Boa *et al.*, 2005), biphenylamides (Baldwin *et al.*, 2005), A771726 (Heikkilä *et al.*, 2006), atovaquone (Hansen *et al.*, 2004), and leflunomide (Hurt *et al.*, 2006) show that all these analogues bind similarly, attacking the ubiquinone binding site formed jointly by the N- and C-terminal domains (Fig. 2C). Unfortunately, given the involvement of the Class 2-specific N-terminal domain, this class of inhibitors is unlikely to be relevant to Class 1 enzymes.

However, inhibitors specific to Class 1A enzymes are also known, including hydroxybenzoates. These are orotate analogues that have been shown to specifically inhibit the *L. lactis* Class 1A DHODH with minimal effect on the *L. lactis* Class 1B enzyme or the human and *E. coli* Class 2 enzymes (Palfey *et al.*, 2001). Although the stereochemistry of the protein residues forming the orotate binding site Class 1A and Class 2 enzymes are nearly identical, the redox mechanism differs in the two classes (Fagan *et al.*, 2007). Fagan *et al.* (2007) have attributed this to subtle dynamic features of the proteins. On the basis of the present structure, we suggest that these features include differential access to the orotate and FMN sites from the 'front' side of the protein (Fig. 2) and a difference in the relative mobility observed crystallographically for residues 132–138 in the pyr-binding motif (Fig. 3).

Wolfe *et al.* (2007) further investigated the structural details and kinetics of hydroxybenzoate inhibition of the *L. lactis* Class 1A DHODH. The inhibitor was observed crystallographically only in one monomer of the homodimer, consistent with kinetic data showing cooperativity between the two monomers of the dimer. The structural basis for this cooperativity is not evident (Wolfe *et al.*, 2007). Given the high structural conservation between the *L. lactis* structure and the present *T. brucei* structure, it seemed plausible that this class of inhibitors was also relevant to trypanosomal homologues. We have now shown through inhibition assays on TbDHODH that hydroxybenzoate inhibitors act indeed not only on bacterial DHODHs but also on this Class 1A DHODH from a eukaryotic parasite. In particular, we found competitive

inhibition by 3,4-dihydroxybenzoate (K_i of 58 μM) and non-competitive inhibition by 3,5-dihydroxybenzoate (K_i of 200 μM). These K_i values are higher than those reported for *L. lactis* but remain possible starting points for anti-parasitic drug design.

Applicability of inhibitor design to other pathogens

Trypanosoma brucei is a representative of a larger class of pathogenic protozoan parasites responsible for a substantial burden of human disease. In evaluating the importance of TbDHODH as a possible drug target, it is therefore of interest whether drugs acting on TbDHODH would also be effective against related pathogens. Class 1A DHODHs are primarily bacterial, although they have been acquired by some yeasts (*Saccharomyces*, *Kluyveromyces*) apparently through lateral gene transfer from *Lactococcus* (Hall *et al.*, 2005). The appearance of Class 1A DHODH also in trypanosomatids may similarly be due to lateral transfer, but the point of introduction into the clade of protozoan lineages is not known.

The sequences of *T. brucei* Class 1A, *L. lactis* Class 1B and *P. falciparum* Class 2 DHODH were submitted to the GeneDB omniBLAST server (Hertz-Fowler *et al.*, 2004) to find homologues in other protozoa. No species was found to contain more than one DHODH class. No protozoan Class 1B homologues were detected. The *Plasmodium* genomes contain only Class 2 sequences. The sequences from *T. brucei*, *T. brucei gambiense*, *T. cruzi*, *T. congolense*, *T. vivax*, *L. major* and *L. infantum* have > 75% sequence identity to the genome strain TbDHODH. The residues involved in binding FMN and orotate are conserved, suggesting that drug design based on the TbDHODH structure is relevant to other pathogenic trypanosomatids.

Summary

We have shown that RNAi interference with DHODH in bloodstream form *T. brucei* inhibits growth when access to pyrimidines in the environment is also blocked. This calls into question the general essentiality of the pyrimidine biosynthesis pathway in *T. brucei*, in distinction to a previous report of essentiality in *T. cruzi*. However, we have also shown that RNAi suppression of DHODH is synergistic with the effect of the complementary growth-blocking agent 5-FU, which inhibits pyrimidine uptake. This demonstrates that interference with *T. brucei* DHODH can potentiate the activity of the established clinical drug 5-FU against bloodstream form *T. brucei*.

The crystal structure and enzymatic properties of the *T. brucei* enzyme show that its active site is more similar to those of other Class 1A DHODHs than to the Class 2 DHODHs of higher eukaryotes, including human DHODH.

Encouragingly, it is inhibited by hydroxybenzoates, in common with other Class 1A DHODHs but in distinction to the Class 2 human DHODH.

Thus *T. brucei* DHODH, and by extension other enzymes on the pyrimidine biosynthetic pathway, remains a possible target for the development of a two-pronged therapeutic approach attacking both pyrimidine biosynthesis and pyrimidine uptake. Furthermore, we propose that the molecular details provided by the present TbDHODH structure may be useful in designing selective inhibitors and potential lead compounds targeting other protozoan DHODHs.

Experimental procedures

Protein expression for crystallography

The gene encoding TbDHODH was PCR amplified from genomic DNA of the strain *T. brucei* TREU927 GUTat 10.1 and cloned into a vector AVA421, which is based on *E. coli* expression vector pET14b (Alexandrov *et al.*, 2004). The AVA421 vector contains a cleavable N-terminal His-tag. The protein was purified using a Ni-NTA column and the bound protein was cleaved by protease 3C overnight at 4°C. The released protein was further purified by gel filtration on a HiLoad Superdex 200.

Protein expression for enzymatic studies

The DHODH gene was amplified from *T. brucei brucei* 427 strain genomic DNA by polymerase chain reaction using the primers 5'-CGCAAAGGGAAAAGTCATATGAGTTTGAAAAGT TAAT-3' and 5'-CATCAACACCCATGTATCTCGAGATCCA TCGTCTTCACGC-3', which introduced NdeI and XhoI restriction sites. The product was subcloned, then ligated into pET22b (EMD Biosciences) providing a C-terminus His-tag. The resulting TbDHODH-pET22b plasmid was then transformed into BL21-DE3 *E. coli* cells, and grown in LB Miller medium to an OD₆₀₀ of 0.8, then supplemented with 100 µM FMN and induced with 200 µM IPTG. A cell pellet was collected 3 h after induction and re-suspended in lysis buffer (50 mM sodium phosphate, pH 8.0, 10 mM imidazole, 5 mM 2-mercaptoethanol, 10% glycerol, 1 mg ml⁻¹ lysozyme, 0.1 mg ml⁻¹ DNase) and a protease inhibitor cocktail was added with a final concentration of 200 µM phenylmethylsulphonyl fluoride, 1 µg ml⁻¹ leupeptin, 2 µg ml⁻¹ antipain, 10 µg ml⁻¹ benzamidin, 1 µg ml⁻¹ pepstatin and 1 µg ml⁻¹ chymostatin. The lysis mixture was then incubated for 2 h on ice with constant stirring, sonicated and centrifuged at 20 000 *g* for 30 min at 4°C. The supernatant from centrifugation was loaded onto a 10 ml column of nickel agarose resin (Qiagen) equilibrated with Wash buffer (50 mM sodium phosphate, pH 8.0, 300 mM sodium chloride, 20 mM imidazole, 5 mM 2-mercaptoethanol, 10% glycerol). The column was washed with 10 volumes of Wash buffer, then His₆-tagged protein was eluted with Elution buffer (50 mM sodium phosphate, pH 8.0, 300 mM sodium chloride, 300 mM imidazole, 5 mM 2-mercaptoethanol, 10% glycerol). The eluted protein was pooled and concentrated to less than 2 ml with a Cen-

triprep YM-10 centrifugal filtration device (Amicon Millipore) and applied to a HiPrep 26/10 Desalting Column (Amersham Biosciences) equilibrated with 50 mM sodium phosphate, pH 8.0, 150 mM sodium chloride, and 10% glycerol. Protein containing fractions were pooled and concentrated as above.

Crystallization

Purified TbDHODH was shipped on dry ice for High Throughput Crystallization Screening at the Hauptman-Woodward Medical Research Institute (Luft *et al.*, 2003). The sample was rapidly thawed in a 30°C water bath and orotic acid (8 µl of a 200 mM orotic acid stock solution) was added to 392 µl of the protein solution. Crystallization experiments were set up using the microbatch-under-oil technique (Chayen *et al.*, 1992) with a Robbins Scientific Tango liquid handling system. Each of the 1536 experiments contained 200 nL of crystallization cocktail solution combined with 200 nL of protein solution under USP grade mineral oil (Sigma cat #M1180) contained in a low birefringence 1536 well microassay plate (Greiner BioOne cat #790801). Manual review of plate images after 1 week at 4°C identified 124 crystallization conditions with outcomes considered suitable for optimization trials. Eight initial hits were optimized and crystals grown by the sitting drop method. Crystals used for data collection grew from a drop consisting of 0.4 µl of protein solution (14.1 mg ml⁻¹), mixed with 0.4 µl of reservoir solution containing 40% PEG 1000, 0.1 M Na citrate, 0.1 M KBr, pH 4.0 at room temperature.

X-ray crystal structure determination and structural analysis

Native crystals were flash frozen directly in liquid nitrogen. Data were collected to 1.95 Å resolution from a single crystal maintained at 100K, at an X-ray wavelength corresponding to the bromine K edge ($\lambda = 0.92010$ Å), on ALS beamline 8.2.1. Data were processed and scaled using MOSFLM and the CCP4 program package (Collaborative Computational Project No. 4, 1994) via the automated Wedger and Scaler scripts of Elves (Holton and Alber, 2004). Data processing statistics are shown in Table 1. The contribution of anomalous dispersion from ordered Br atoms to the measured Bragg intensities was insufficient to solve the structure using SAD phasing, although 11 partially occupied sites were later identified in the refined structure. Therefore, the structure of *L. lactis* DHODH (PDB accession code 1jue, 51% sequence identity) was submitted to the Swiss model server (Guex and Peitsch, 1997; Schwede *et al.*, 2003) to create a hybrid homology model based upon the structure of *L. lactis* DHODH but containing the TbDHODH residues. This model was submitted to Molrep (Vagin and Teplyakov, 1997), which placed four copies of the monomeric model into the asymmetric unit yielding a correlation coefficient 0.60. The TbDHODH structure was refined using Refmac5 (Murshudov *et al.*, 1997) against all reflections between 21 and 1.95 Å resolution, keeping 5% of the reflections for R_{free}. Model building and validation were accomplished using Coot (Emsley and Cowtan, 2004) and Molprobability (Lovell *et al.*, 2003). Electron density in the region of the orotate binding site is shown

Table 1. Crystallographic data collection, phasing and refinement statistics.

Data collection	
Wavelength (Å)	0.92010
Resolution (Å)	21–1.95 (2.06–1.95)
Space group	C222 ₁
Unit cell (Å)	a = 81.6, b = 162.6, c = 163.1
Total number of observations	336 695 (22 749)
Unique reflections	76 097 (9174)
R _{sym}	0.107 (0.428)
Completeness (%)	96.2 (80.2)
I/σ(I)	7.5 (1.8)
Redundancy	4.4 (2.5)
Wilson B factor (Å ²)	25.5
Refinement	
Resolution (Å)	21–1.95
R/R _{free}	0.189/0.242
Rmsd bonds (Å)	0.011
Rmsd angles (°)	1.326
Mean B protein (Å ²)	15.2
Mean B orotate, FMN (Å ²)	11.7
Mean B other atoms (Å ²)	19.8
Residues with φ,ψ in most favoured regions (%)	91.3
Residues with φ,ψ in allowed regions (%)	8.7
Residues with φ,ψ in disallowed regions	0

in Fig. S5. The final model consists of four molecules forming two dimers. The final model for each monomer consists of residues 1–313, one orotate and one FMN molecule. The overall model also contains 11 bromide atoms, three glycerol molecules and 638 water molecules. The final model and crystallographic structure factors have been deposited with the Protein Data Bank (accession code 2b4g).

Enzyme kinetic and inhibition assays

Enzyme kinetic assays were performed in enzyme assay buffer (50 mM HEPES, pH 8.0, 150 mM NaCl, 10% glycerol) at 25°C. Analysis of pH dependence utilized MES (pH 5.5–6.5), MOPS (pH 6.5–7.5), Tris (pH 7.5–9.0) or CHES (pH 9.0–10.0) buffer salts in place of HEPES. Production of orotate was monitored at 300 nm ($\epsilon_{300} = 2.65 \text{ mM}^{-1}\text{cm}^{-1}$) when using fumarate, at 282 nm ($\epsilon_{282} = 6.60 \text{ mM}^{-1}\text{cm}^{-1}$) when using vitamin K analogues, and at 296 nm ($\epsilon_{296} = 4.30 \text{ mM}^{-1}\text{cm}^{-1}$) when using ubiquinone analogues. Reduction of NAD⁺ was monitored at 340 nm ($\epsilon_{340} = 6.22 \text{ mM}^{-1}\text{cm}^{-1}$). Strong absorption in the far-UV by the inhibitors tested required the use of the traditional electron acceptor dichlorophenolindophenol (DCIP) in inhibition studies where reduction of DCIP was followed at 600 nm ($\epsilon_{600} = 18.8 \text{ mM}^{-1}\text{cm}^{-1}$).

DHO-dependent activity was examined in the presence of 500 μM fumarate. Fumarate-dependent activity was assayed at a constant DHO concentration of 250 μM . Data were analysed using the software package GraphPad Prism and SigmaPlot and fitted to the Michaelis–Menten equation.

Alternative electron acceptors (vitamin K and ubiquinone analogues, NAD⁺) were assayed at 100 μM electron acceptor (dissolved oxygen was estimated to be ~210 μM) and 250 μM

DHO. Inhibitors were initially examined at 1 mM in the presence of 25 μM DHO and 120 μM DCIP, and subsequent assays utilized 120 μM DCIP, various DHO and inhibitor concentrations. All experiments were performed in at least duplicate; combined data are presented, and kinetic parameters are reported as the mean \pm standard error of the fit.

Analytical ultracentrifugation

Analytical ultracentrifugation was performed on a Beckman XL-I analytical ultracentrifuge and enzyme was observed at 280 nm (protein) and 454 nm (FMN). Enzyme samples of 5–25 μM were centrifuged at 14 000 and 20 000 r.p.m. at 4°C, equilibrium sedimentation scans were obtained every two hours, and equilibrium was determined to be reached when contiguous scans were indistinguishable. Data were fitted to both a single ideal species model and a monomer-dimer model and one representative result from multiple experiments is presented.

RNA interference

A region of the TbDHODH gene sequence was selected for RNAi using the program RNAi (Redmond *et al.*, 2003). Bases 413–859 of the gene were amplified from *T. brucei* 927 genomic DNA using the primers 5'-ATACCAATGTGATGGC ACAGGTCGGATATGACTTTGA-3' and 5'-ATACCATAGAGT TGGGTTGAGTCGAGCAAATATGATG-3'. The amplicon was ligated using TA cloning into the vector pGEM-T (Promega, cat #A3600), then excised with the enzyme BstXI. This insert was ligated into the stem-loop RNAi vector, pQuadra3, as described elsewhere (Inoue *et al.*, 2005). The construct was sequenced to verify the identity of the insert, then linearized with NotI in preparation for electroporation.

Trypanosoma brucei bloodstream-form parasites expressing the T7 RNA polymerase and the Tet repressor under a single selection marker were provided by G. Cross (Rockefeller University) (Wirtz *et al.*, 1999). The cells were grown in HMI-9 with 10% heat-inactivated fetal bovine serum at 37°C and 5% CO₂ with G418 at 2.5 $\mu\text{g ml}^{-1}$ (Hirumi and Hirumi, 1989). Mid-log phase *T. brucei* (2.5×10^7) were suspended in 500 μl of cytomix (120 mM KCl, 0.15 mM CaCl₂, 10 mM K₂HPO₄/KH₂PO₄ pH 7.6, 25 mM HEPES, 2 mM Na₂EDTA, 5 mM MgCl₂) containing 10 μg of NotI linearized pQuadra3/DHODH DNA. The mixture was electroporated in a 4 mm gap cuvette with 1.6 kV and 24 Ω resistance. Cells were re-suspended in HMI-9 medium in the presence of 2.5 $\mu\text{g ml}^{-1}$ phleomycin and 2.5 $\mu\text{g ml}^{-1}$ G418. Individual clones were selected for subsequent RNAi studies. The expression of dsRNA was induced by addition of 1 $\mu\text{g ml}^{-1}$ tetracycline to the cultures diluted to 1×10^5 cells ml^{-1} . Cultures were passed at a 1:10–1:20 dilution daily and cell concentrations were monitored using a ATPLite Luminescence ATP detection Assay System (PerkinElmer, cat #6016941).

Separate growth experiments were performed using HMI-9 medium that omitted thymidine (normally included at 16 μM). There are no other pyrimidine bases in the medium; it is supplemented with 100 μM hypoxanthine as a source of purines. The medium was supplemented with 10% dialysed fetal bovine serum (Hyclone) to complete the pyrimidine depleted medium.

Northern analysis

RNA was isolated from induced and non-induced cultures after 72 h of growth using a RNEasy kit (Qiagen). Sixteen micrograms of total RNA was electrophoresed on a formaldehyde gel and blotted using standard procedures. The RNA membrane was then analysed with a DNA probe amplified from genomic DNA using the primers 5'-CTCGGACA TGAGTTTTCCAACC-3' and 5'-GGCTTCCTACTGTAATCG TGCG-3' that correspond to bases 22–281 of the DHODH open reading frame. The blot was stripped and re-probed with DNA of the *T. brucei* β -tubulin gene for standardization.

IC₅₀ shift assay

Sensitivity to 5-FU was tested against trypomastigotes of the single marker parent line and the single marker cells containing the pQuadra3/DHODH RNAi vector in both uninduced cells and cells induced for 48 h with 1 $\mu\text{g ml}^{-1}$ tetracycline. Cells were added to 96-well plates in triplicate with an initial inoculum of 2×10^4 trypomastigotes per well. The compound stock solution of 5-FU (Sigma, F6627) was prepared using sterile water at an initial concentration of 20 mM. This was diluted in HMI-9 to a concentration of 120 μM and added in serial dilutions for a final volume of 200 μl per well. Parasite growth was quantified at 48 h by the addition of Alamar Blue (Alamar Biosciences, DAL1100) (Raz *et al.*, 1997).

5-FU incorporation experiment

Incorporation of 5-FU into *T. brucei* genomic DNA was measured for the bloodstream forms of the single marker parent cell line and for the bloodstream forms containing the pQuadra3/DHODH RNAi construct. Measurements were taken for both uninduced cultures and cultures that had been induced for 72 h with 1 $\mu\text{g ml}^{-1}$ tetracycline. The trypomastigotes were all grown in standard HMI-9 containing thymidine and hypoxanthine, as well as 2.5 $\mu\text{g ml}^{-1}$ neomycin. In addition, the cells containing the pQuadra3/DHODH RNAi vector were also grown in the presence of 2.5 $\mu\text{g ml}^{-1}$ pleomycin. After the 72 h induction, cells were transferred to a 96-well plate and pulsed with 5 μCi of [6-³H]-5-FU (Moravek Biochemicals, MT-686) for 24 h. Cell density quantification, in order to standardize results, was carried out with 30 μl of sample using the ATPLite Luminescence ATP detection Assay System (PerkinElmer, cat #6016941) as described above. The incorporation of ³H-5-FU was measured by binding the DNA from the remaining 175 μl onto glass fibre filters with a cell harvester (Inotech Biosystems International, Rockville, MD, USA), and the radioactivity incorporated into the parasites was counted on a Chameleon 425–104 multilabel plate scintillation counter (Hidex Oy, Turku, Finland).

Antibody production and Western immunoblotting

Purified TbDHODH was sent to Affinity BioReagents (Golden, CO) for antibody production in rabbits as previously described. Antibody specificity was confirmed against

purified TbDHODH and *T. brucei* cells lysates using preimmune and post-challenge serum and found to be specific. The anti-TbDHODH antibodies were used in Western blots on lysates of *T. brucei* bloodstream form cells collected before and at daily time intervals after induction of RNAi. Standard Western blot procedures were followed using goat-horseradish peroxidase-conjugated secondary antibody and ECL detection (Amersham Biosciences). Relative TbDHODH protein levels were determined by densitometry. The numerical values were normalized to stained bands from the transferred SDS-PAGE gel (not shown).

Acknowledgements

We thank Jonathan Caruthers and Meg Holmes for aid in data collection. We are also reliant on the efforts of other members of the SGPP consortium, including Eric Phizicky, Erin Quartley, Angela Lauricella, Lori Schoenfeld, Jennifer Ross, Frank Zucker and Thomas Earnest. We thank Dr HP de Koning for helpful discussions about *T. brucei* transporter activities. This work was supported by the Protein Structure Initiative, award NIGMS GM64655; NIH award AI067921; funds from the Howard Hughes Medical Institute (HHMI) to WGJH; and by the National Institutes of Health Grants AI053680 to MAP. Portions of this work were carried out at the Advanced Light Source, which is supported by the Director, Office of Science, Office of Basic Energy Sciences, of the US Department of Energy under Contract No. DE-AC02-05CH11231.

References

- Alexandrov, A., Vignali, M., LaCount, D.J., Quartley, E., de Vries, C., Rosa, D.D., *et al.* (2004) A facile method for high-throughput co-expression of protein pairs. *Mol Cell Proteomics* **3**: 934–938.
- Andersen, P.S., Jansen, P.J., and Hammer, K. (1994) Two different dihydroorotate dehydrogenases in *Lactococcus lactis*. *J Bacteriol* **176**: 3975–3982.
- Annoura, T., Nara, T., Makiuchi, T., Hashimoto, T., and Aoki, T. (2005) The origin of dihydroorotate dehydrogenase genes of kinetoplastids, with special reference to their biological significance and adaptation to anaerobic, parasitic conditions. *J Mol Evol* **60**: 113–127.
- Baldwin, J., Michnoff, C.H., Malmquist, N.A., White, J., Roth, M.G., Rathod, P.K., and Phillips, M.A. (2005) High-throughput screening for potent and selective inhibitors of *Plasmodium falciparum* dihydroorotate dehydrogenase. *J Biol Chem* **280**: 21847–21853.
- Beitz, E. (2000) TEXshade: shading and labeling of multiple sequence alignments using LATEX2 epsilon. *Bioinformatics* **16**: 135–139.
- Berriman, M. (2004) Data mining parasite genomes. *Parasitology* **128** (Suppl.): S23–S31.
- Boa, A.N., Canavan, S.P., Hirst, P.R., Ramsey, C., Stead, A.M.W., and McConkey, G.A. (2005) Synthesis of brequinar analogue inhibitors of malaria parasite dihydroorotate dehydrogenase. *Bioorg Med Chem* **13**: 1945–1967.
- de Bono, J.S., and Twelves, C.J. (2001) The oral fluorinated pyrimidines. *Invest New Drugs* **19**: 41–59.

- Chaudhary, K., and Roos, D.S. (2005) Protozoan genomics for drug discovery. *Nat Biotechnol* **23**: 1089–1091.
- Chayen, N.E., Stewart, P.D.S., and Blow, D.M. (1992) Microbatch crystallization under oil – a new technique allowing many small-volume crystallization trials. *J Cryst Growth* **122**: 176–180.
- Collaborative Computational Project, No. 4 (1994) The ccp4 suite: programs for protein crystallography. *Acta Crystallogr D* **50**: 760–763.
- Emsley, P., and Cowtan, K. (2004) Coot: model-building tools for molecular graphics. *Acta Crystallogr D* **60**: 2126–2132.
- Fagan, R., Jensen, K., Bjornberg, O., and Palfey, B. (2007) Mechanism of flavin reduction in the class 1A dihydroorotate dehydrogenase from *Lactococcus lactis*. *Biochemistry* **46**: 4028–4036.
- Feliciano, P.R., Cordeiro, A.T., Costa-Filho, A.J., and Nonato, M.C. (2006) Cloning, expression, purification, and characterization of *Leishmania major* dihydroorotate dehydrogenase. *Protein Expr Purif* **48**: 98–103.
- Guda, C., Lu, S., Scheeff, E.D., Bourne, P.E., and Shindyalov, I.N. (2004) CE-MC: a multiple protein structure alignment server. *Nucleic Acids Res* **32**: W100–W103.
- Gudin, S., Quashie, N.B., Candlish, D., Al-Salabi, M.I., Jarvis, S.M., Ranford-Cartwright, L.C., and de Koning, H.P. (2006) *Trypanosoma brucei*: a survey of pyrimidine transport activities. *Exp Parasitol* **114**: 118–125.
- Guex, N., and Peitsch, M.C. (1997) SWISS-MODEL and the Swiss-PdbViewer: an environment for comparative protein modeling. *Electrophoresis* **18**: 2714–2723.
- Hall, C., Brachat, S., and Dietrich, F.S. (2005) Contribution of horizontal gene transfer to the evolution of *Saccharomyces cerevisiae*. *Eukaryot Cell* **4**: 1102–1115.
- Hansen, M., Nours, J.L., Johansson, E., Antal, T., Ullrich, A., Löffler, M., and Larsen, S. (2004) Inhibitor binding in a class 2 dihydroorotate dehydrogenase causes variations in the membrane-associated N-terminal domain. *Protein Sci* **13**: 1031–1042.
- Heikkilä, T., Thirumalairajan, S., Davies, M., Parsons, M.R., McConkey, A.G., Fishwick, C.W.G., and Johnson, A.P. (2006) The first *de novo* designed inhibitors of *Plasmodium falciparum* dihydroorotate dehydrogenase. *Bioorg Med Chem Lett* **16**: 88–92.
- Hertz-Fowler, C., Peacock, C.S., Wood, V., Aslett, M., Kerhornou, A., Mooney, P., *et al.* (2004) GeneDB: a resource for prokaryotic and eukaryotic organisms. *Nucleic Acids Res* **32**: D339–D343.
- Hirumi, H., and Hirumi, K. (1989) Continuous cultivation of *Trypanosoma brucei* blood stream forms in a medium containing a low concentration of serum protein without feeder cell layers. *J Parasitol* **75**: 985–989.
- Holton, J., and Alber, T. (2004) Automated protein crystal structure determination using ELVES. *Proc Natl Acad Sci USA* **101**: 1537–1542.
- Hurt, D.E., Widom, J., and Clardy, J. (2006) Structure of *Plasmodium falciparum* dihydroorotate dehydrogenase with a bound inhibitor. *Acta Crystallogr D Biol Crystallogr* **62**: 312–323.
- Inaoka, D.K., Takashima, E., Osanai, A., Shimizu, H., Nara, T., Aoki, T., *et al.* (2005) Expression, purification and crystallization of *Trypanosoma cruzi* dihydroorotate dehydrogenase complexed with orotate. *Acta Crystallogr Sect F Struct Biol Cryst Commun* **61**: 875–878.
- Inoue, M., Nakamura, Y., Yasuda, K., Yasaka, N., Hara, T., Schnauffer, A., *et al.* (2005) The 14–3–3 proteins of *Trypanosoma brucei* function in motility, cytokinesis, and cell cycle. *J Biol Chem* **280**: 14085–14096.
- Karibian, D. (1978) Dihydroorotate dehydrogenase (*Escherichia coli*). *Methods Enzymol* **51**: 58–63.
- Knecht, W., Bergjohann, U., Gonski, S., Kirschbaum, B., and Löffler, M. (1996) Functional expression of a fragment of human dihydroorotate dehydrogenase by means of the baculovirus expression vector system, and kinetic investigation of the purified recombinant enzyme. *Eur J Biochem* **240**: 292–301.
- de Koning, H.P., and Jarvis, S.M. (1998) A highly selective, high-affinity transporter for uracil in *Trypanosoma brucei*: evidence for proton-dependent transport. *Biochem Cell Biol* **76**: 853–858.
- Laskowski, R.A., Chistyakov, V.V., and Thornton, J.M. (2005) PDBsum more: new summaries and analyses of the known 3D structures of proteins and nucleic acids. *Nucleic Acids Res* **33**: D266–D268.
- Liu, S., Neidhardt, E.A., Grossman, T.H., Ocain, T., and Clardy, J. (2000) Structures of human dihydroorotate dehydrogenase in complex with antiproliferative agents. *Structure* **8**: 25–33.
- Lovell, S.C., Davis, I.W., Arendall, W.B., de Bakker, P.I.W., Word, J.M., Prisant, M.G., *et al.* (2003) Structure validation by Calpha geometry: phi, psi and Cbeta deviation. *Proteins* **50**: 437–450.
- Luft, J.R., Collins, R.J., Fehrman, N.A., Lauricella, A.M., Veatch, C.K., and DeTitta, G.T. (2003) A deliberate approach to screening for initial crystallization conditions of biological macromolecules. *J Struct Biol* **142**: 170–179.
- Marcinkeviciene, J., Jiang, W., Locke, G., Kopcho, L.M., Rogers, M.J., and Copeland, R.A. (2000) A second dihydroorotate dehydrogenase (Type A) of the human pathogen *Enterococcus faecalis*: expression, purification, and steady-state kinetic mechanism. *Arch Biochem Biophys* **377**: 178–186.
- McRobert, L., and McConkey, G.A. (2002) RNA interference (RNAi) inhibits growth of *Plasmodium falciparum*. *Mol Biochem Parasitol* **119**: 273–278.
- Murshudov, G.N., Vagin, A.A., and Dodson, E.J. (1997) Refinement of macromolecular structures by the maximum-likelihood method. *Acta Crystallogr D* **53**: 240–255.
- Nara, T., Hshimoto, T., and Aoki, T. (2000) Evolutionary implications of the mosaic pyrimidine-biosynthetic pathway in eukaryotes. *Gene* **257**: 209–222.
- Nielsen, F.S., Andersen, P.S., and Jensen, K.F. (1996a) The B form of dihydroorotate dehydrogenase from *Lactococcus lactis* consists of two different subunits, encoded by the pyrDb and pyrK genes, and contains FMN, FAD, and [FeS] redox centers. *J Biol Chem* **271**: 29359–29365.
- Nielsen, F.S., Rowland, P., Larsen, S., and Jensen, K.F. (1996b) Purification and characterization of dihydroorotate dehydrogenase A from *Lactococcus lactis*, crystallization and preliminary X-ray diffraction studies of the enzyme. *Protein Sci* **5**: 852–856.
- Nørager, S., Arent, S., Björnberg, O., Ottosen, M., Leggio,

- L.L., Jensen, K.F., and Larsen, S. (2003) *Lactococcus lactis* dihydroorotate dehydrogenase A mutants reveal important facets of the enzymatic function. *J Biol Chem* **278**: 28812–28822.
- Palfey, B.A., Björnberg, O., and Jensen, K.F. (2001) Specific inhibition of a family 1A dihydroorotate dehydrogenase by benzoate pyrimidine analogues. *J Med Chem* **44**: 2861–2864.
- Papageorgiou, I.G., Yakob, L., Salabi, M.I.A., Diallinas, G., Soteriadou, K.P., and Koning, H.P.D. (2005) Identification of the first pyrimidine nucleobase transporter in *Leishmania*: similarities with the *Trypanosoma brucei* U1 transporter and antileishmanial activity of uracil analogues. *Parasitology* **130**: 275–283.
- Raz, B., Iten, M., Grether-Buhler, Y., Kaminsky, R., and Brun, R. (1997) The Alamar Blue assay to determine drug sensitivity of African trypanosomes (*T.b. rhodesiense* and *T.b. gambiense*) *in vitro*. *Acta Trop* **68**: 139–147.
- Redmond, S., Vadivelu, J., and Field, M.C. (2003) RNAi: an automated web-based tool for the selection of RNAi targets in *Trypanosoma brucei*. *Mol Biochem Parasitol* **128**: 115–118.
- Rowland, P., Nørager, S., Jensen, K.F., and Larsen, S. (2000) Structure of dihydroorotate dehydrogenase B: electron transfer between two flavin groups bridged by an iron-sulphur cluster. *Structure* **8**: 1227–1238.
- Schwede, T., Kopp, J., Guex, N., and Peitsch, M.C. (2003) SWISS-MODEL: an automated protein homology-modeling server. *Nucleic Acids Res* **31**: 3381–3385.
- Takashima, E., Inaoka, D.K., Osanai, A., Nara, T., Odaka, M., Aoki, T., et al. (2002) Characterization of the dihydroorotate dehydrogenase as a soluble fumarate reductase in *Trypanosoma cruzi*. *Mol Biochem Parasitol* **122**: 189–200.
- Vagin, A., and Teplyakov, A. (1997) Molrep: an automated program for molecular replacement. *J Appl Cryst* **30**: 1022–1025.
- Wang, C.C. (1997) Validating targets for antiparasite chemotherapy. *Parasitology* **114** (Suppl.): S31–44.
- Wirtz, E., Leal, S., Ochatt, C., and Cross, G.A. (1999) A tightly regulated inducible expression system for conditional gene knock-outs and dominant-negative genetics in *Trypanosoma brucei*. *Mol Biochem Parasitol* **99**: 89–101.
- Wolfe, A., Thymark, M., Gattis, S., Fagan, R., Hu, Y.-C., Johansson, E., et al. (2007) Interaction of benzoate pyrimidine analogues with class 1A dihydroorotate dehydrogenase from *Lactococcus lactis*. *Biochemistry* **46**: 5741–5753.

Supplementary material

This material is available as part of the online article from: <http://www.blackwell-synergy.com/doi/abs/10.1111/j.1365-2958.2008.06131.x>
(This link will take you to the article abstract).

Please note: Blackwell Publishing is not responsible for the content or functionality of any supplementary materials supplied by the authors. Any queries (other than missing material) should be directed to the corresponding author for the article.